OPEN ACCESS
IOP Publishing
Classical and Quantum Gravity
Class. Quantum Grav. **42** (2025) 185003 (13pp)
https://doi.org/10.1088/1361-6382/adfffa

AthenaK simulations of the binary black hole merger GW150914

David Radice[1,2,3,7,*], **Rossella Gamba**[1,2,4], **Hengrui Zhu**[5,6] **and Alireza Rashti**[1,2]

[1] Institute for Gravitation & the Cosmos, The Pennsylvania State University, University Park, PA 16802, United States of America
[2] Department of Physics, The Pennsylvania State University, University Park, PA 16802, United States of America
[3] Department of Astronomy & Astrophysics, The Pennsylvania State University, University Park, PA 16802, United States of America
[4] Department of Physics, University of California, Berkeley, CA 94720, United States of America
[5] Department of Physics, Princeton University, Jadwin Hall, Washington Road, Princeton, NJ 08544, United States of America
[6] Princeton Gravity Initiative, Princeton University, Princeton, NJ 08544, United States of America

E-mail: dur566@psu.edu

Received 7 June 2025; revised 15 August 2025
Accepted for publication 27 August 2025
Published 11 September 2025

Abstract

We present new binary black hole simulations targeted to GW150914 using the GPU-accelerated code `AthenaK`. We compute the properties of the final remnant with the isolated horizon formalism and obtain gravitational-waveforms at future null infinity via Cauchy characteristic extraction. We compare our results with those obtained by the Simulating eXtreme Spacetimes (SXS) and Rochester Institute of Technology (RIT) groups, targeted to the same event. We find excellent agreement with the SXS and RIT results in the remnant mass, spin, and recoil velocity. For the dominant $(\ell, m) = (2, 2)$ mode of the gravitational-wave signal we find maximum dephasing of $\Delta\phi \simeq 0.35$ and amplitude difference of $\Delta A/A \simeq 0.4\%$. We use our newly computed waveform to

[7] Alfred P. Sloan Fellow.
[*] Author to whom any correspondence should be addressed.

re-analyze the GW150914 data and find posteriors for chirp mass, luminosity distance, and inclination that are broadly consistent with those obtained using semi-analytic waveform models. This work demonstrates the viability of `AthenaK` for many-orbits binary black hole merger simulations. A step-by-step tutorial, including all necessary input files and analysis scripts to reproduce our results, is available on `GitHub`.

Keywords: numerical relativity, gravitational-wave astronomy, GW150914

1. Introduction

The detection of the gravitational-wave (GW) signal GW150914 from a binary black hole (BBH) merger by the LIGO observatories in Hanford (WA) and Livingston (LA) opened a new window on the Universe and ushered in the era of GW astronomy [1–3]. This discovery was recognized with the 2017 Physics Nobel Prize to Rainer Weiss, Barry C. Barish, and Kip S. Thorne. GW150914 confirmed the predictions of Einstein's general relativity in the strong field regime [4–7], for example by enabling tests of the no hair theorem [8–11] and of the BH area law [12, 13].

Numerical relativity (NR) played a key role in this discovery, as it provides the only way to calculate the complete waveform for merging BHs from first principles [14]. Indeed, the need for large scale numerical computation to solve the two-body problem in general relativity was recognized already in the '70 s with the pioneering work of Smarr *et al* [15]. However, a concerted effort by a large community was necessary to achieve the BBH breakthrough of the early 2000's [16–21]. These early calculations revealed that the GW signal from BBH systems smoothly transitions from the inspiral portion, which is well described by post-Newtonian theory, to the ringdown, which is well described by BH perturbation theory. The merger waveform itself was shown to be stunningly simple as it smoothly blends the inspiral waveform to the ringdown signal. Since then, NR simulations have since significantly increased in sophistication and accuracy [22–34], enabling the calibration of analytic waveform models, such as the effective-one-body [35–45] and phenomenological inspiral-merger-ringdown models [46–62], as well as purely data-driven models [63–67]. Large catalogs of waveforms have been produced and are continuously expanded as progressively larger regions of the binary parameter space are explored [68–79].

Shortly after the announcement of GW150914, Lovelace and collaborators [80] presented NR simulations targeted to the event performed with two independent NR codes: `LazEV` [17, 81] and `SpEC` [23, 30] representing state-of-the-art implementations of the two most successful approaches for the BBH problem. The former implements the Baumgarte, Shapiro, Shibata, Nakamura (BSSN) formalism for the Einstein equations [82–84] with moving puncture gauge [17, 18, 85–87], while the latter implements the generalized-harmonic formalism [88] with singularity excision. Lovelace *et al* [80] demonstrated the excellent agreement between the theory predictions and between theory and experimental results, further establishing the interpretation of the signal GW150914 as being the result of a BBH merger.

In this work, we revisit GW150914 using the new open source code `AthenaK` [89–91], showcasing the capabilities of new-generation NR codes. While `AthenaK` is similar to `LazEV` in many ways, for example, in its use of the moving-puncture gauge, it also includes new developments. `AthenaK` uses the Z4c formulation of Einstein equations [92, 93], which has been shown to result in better constraint preservation and accuracy compared to the original BSSN method. Most importantly, `AthenaK` is designed to run efficiently and at scale on large, GPU-accelerated machines, which are $\sim$100 times faster than leadership scale machines available

in 2016. AthenaK development is fully public [94] and we welcome contributions from the broader community. This paper is accompanied by a detailed step-by-step tutorial and a set of scripts needed to reproduce all simulations and results presented here [95], in the hope of further broadening participation in the NR community.

The rest of this paper is organized as follows. We summarize the numerical techniques implemented in AthenaK and provide details on our initial data in section 2. Our results, as well as comparison with the data from [80] and a direct application to data analysis, are presented in section 3. Finally, section 4 is dedicated to discussion and conclusion. Unless otherwise stated, all quantities are given in natural units in which $M = G = 1$, where M is the binary mass.

2. Methods

The computational kernels in AthenaK have been ported from GR-Athena++ [31] and are summarized in [90], where the differences with GR-Athena++ are also discussed in detail. Here, we summarize the main feature of the code as they pertain the results presented here, but we refer to the previously mentioned works for more details.

We construct initial data using the pseudo-spectral elliptic solver TwoPunctures code [96]. The parameters from the initial data are taken from [80] to match that used for the LazEV code. The Z4c equations are discretized in space using 6th order finite differencing, with advective derivatives along the shift vector β^i lopsided by one grid point. The equations are then evolved in time with a low-storage 4th order Runge–Kutta method. Our computational grid covers a region with extent $[-2048, 2048]^3$. The base grid is covered with 128 points in each direction. To resolve the punctures, we employ 12 levels of adaptive mesh refinement (AMR; including the base grid), with the highest resolution region placed according to the position of the punctures. This results in a finest resolution of $\Delta = 0.007\,8125\,M$ corresponding to $\sim$128 points across the coordinate diameter of each BH, after the initial relaxation of the gauge. Note that, because of the octree block-tree based nature of the AthenaK AMR, this results in a refinement structure that extends throughout the domain. However, we also enforce a minimum resolution of $\Delta = 0.25\,M$ within a (coordinate) radius $r = 200\,M$ to ensure that GWs are well resolved at the radii where we extract them $r \in \{25, 50, 100, 150, 200\}\,M$. The amplitude peak in the $(\ell, m) = (2, 2)$ mode is reached at $t \simeq 2154\,M$, but we continue the simulations until time $2500\,M$. The total wall clock time was of $\sim$130 hours on 32 nodes of ALCF's Aurora (192 GPUs).

We extract GWs in two ways. First, we output the spin weighted multipolarly decomposed complex scalar Ψ_4 on spheres at different radii, e.g. [97]. This data is then integrated twice in time using the fixed-frequency integration method [98] to obtain the strain data in the transverse-traceless gauge. This approach closely follow that of the LazEV team in [80]. The other approach is through Cauchy-characteristic extraction [26, 99–103]. To this aim, we output metric data on a cylinder with $49\,M \leqslant r \leqslant 51\,M$, as outlined in [34]. We then use the open-source code SpECTRE [104] to compute waveforms at $\mathcal{I}^+$. We use the scri package [105] to transform the resulting waveform to the super rest frame of the binary at a time shortly after the end of the junk radiation [106–111]. Scripts to convert AthenaK data to the format needed by SpECTRE are included in [95]. In this work, we focus on the CCE data, which is free from finite-radius extraction artifacts and can also include GW memory effects. A detailed comparison between wave-extraction methods can be found in [34, 102, 112].

AthenaK does not include an apparent horizon finder, however we record 3D metric data in Cartesian boxes with diameter $4\,M$ centered at the location of the punctures. This data is then processed using AHFinderDirect [113] and QuasiLocalMeasures [114] from the

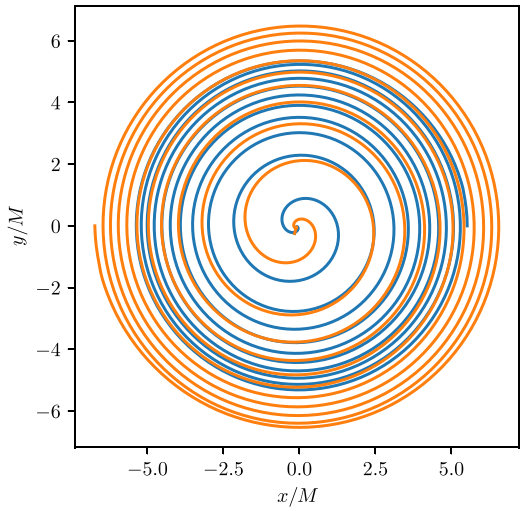

Figure 1. Puncture trajectories obtained by integrating $\dot{x}^i_A = -\beta^i(x_A)$. The primary BH's trajectory is in blue, while the secondary BH trajectory is in orange. The eccentricity of the orbit, estimated from the trajectory, is $e = 8.3 \times 10^{-4}$.

`Einstein Toolkit` [115]. The minimal subset of the `Einstein Toolkit` used for our analysis was developed in the context of the `BlackHoles@Home` project [116].

3. Results

3.1. Dynamics and remnant properties

Our simulation starts from a coordinate separation of $11.8\,M$, corresponding to initial instantaneous orbital frequency of $M\omega = 0.20$, and evolve to merger in $\sim 2050\,M$ over ~ 10 orbits. Figure 1 shows the trajectories of the two punctures from our simulation. We do not observe a significant drift of the center of mass of the system: by the time that the ringdown waveform has decayed to below the numerical noise () the coordinate position of the center of mass has moved only by $0.1\,M$ from the center (about 12 grid points).$t \simeq 2100\,M$ The eccentricity, estimated from the puncture trajectories following the approach described in [117, 118], is . This estimate is obtained by fitting a post-Newtonian expression for the orbital separation to the puncture's coordinate distance starting at $e = 8.3 \times 10^{-4}$ $t = 100\,M$ and extending until the separation drops below $8\,M$. such, e should be taken as a measurement of eccentricity around $M\omega \sim 0.2$. Note that the BHs spins are aligned to the orbital angular momentum, so no precession is present in the evolution.

Figure 2 shows the conformal factor on the orbital plane at the approximate time of merger. At this time a common apparent horizon has already been formed. The mass and dimensionless spin parameters of the remnant, computed using the isolated horizon formalism [119], are $M = 0.951\,948$ and $\chi = J/M^2 = 0.691\,914$. The relative difference with the highest resolution `SpEC` results reported in [80] are of 9×10^{-5} and 2×10^{-4}, respectively. These imply that 4.81% of the initial binary mass is radiated in GWs, consistent with analytic and other numerical predictions [1, 2, 80]. The recoil velocity of the remnant BH, estimated assuming momentum conservation and integrating the momentum flux in GWs with the Cauchy

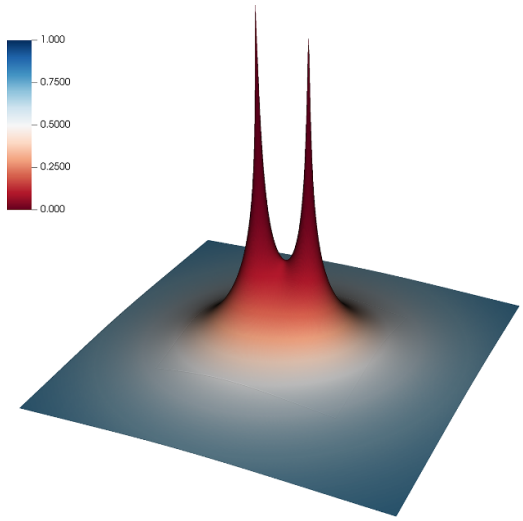

Figure 2. Conformal factor $\chi = \gamma^{-3}$, γ being the determinant spatial metric, at the approximate time of merger $t = 2050\,M$.

characteristic extraction (CCE) data, is of 138.68 km s^{-1}, in good agreement with [80], as it is within 3% of the highest resolution SpEC results.

3.2. *Waveform and comparison against other catalogs*

A selection of waveform multipoles, extrapolated to $\mathcal{I}^+$ via CCE, is shown in figure 3. Our waveforms, notably, contain memory effects (see e.g. [120] for a review), which are especially apparent in the $m = 0$ modes shown. Such effects would cause a displacement in the arms of a detector after a GW has passed through. In our modes, they appear as a 'global offset' that slowly grows during the inspiral, and does not taper to zero beyond merger. One additional feature related to memory is visible in the imaginary part of the $\ell = 3, m = 0$ mode: this is the so-called 'spin memory' effect, related to the change in relative separation of observers with initial relative velocity [109, 121]. It is possible to see noise events in our GW strain data, a prominent example is around $t = 750\,M$ in the h_{40} mode. This noise is possible due to back scattering of waves at AMR boundaries towards the extraction radius. A comparison with data from a higher resolution AthenaK simulation is discussed in appendix.

Figure 4 presents a time domain phasing comparison between the dominant quadrupolar mode obtained in this work and the same quantity extracted from the SXS:BBH:305 and RIT:BBH:0062 simulations, which are respectively the highest resolution calculations obtained with SpEC and LazEV of [80]. Following e.g. [34] we align the modes between the times t_i, t_f demarcated by vertical dotted lines. This is done by determining the time and phase shifts $(\Delta t, \Delta\phi)$ such that the following quantity

$$\chi^2 = \int_{t_i}^{t_f} \left[\phi_{\rm X}\left(t + \Delta t\right) - \phi_{\rm AthenaK} - \Delta\phi\right]^2 {\rm d}t \tag{1}$$

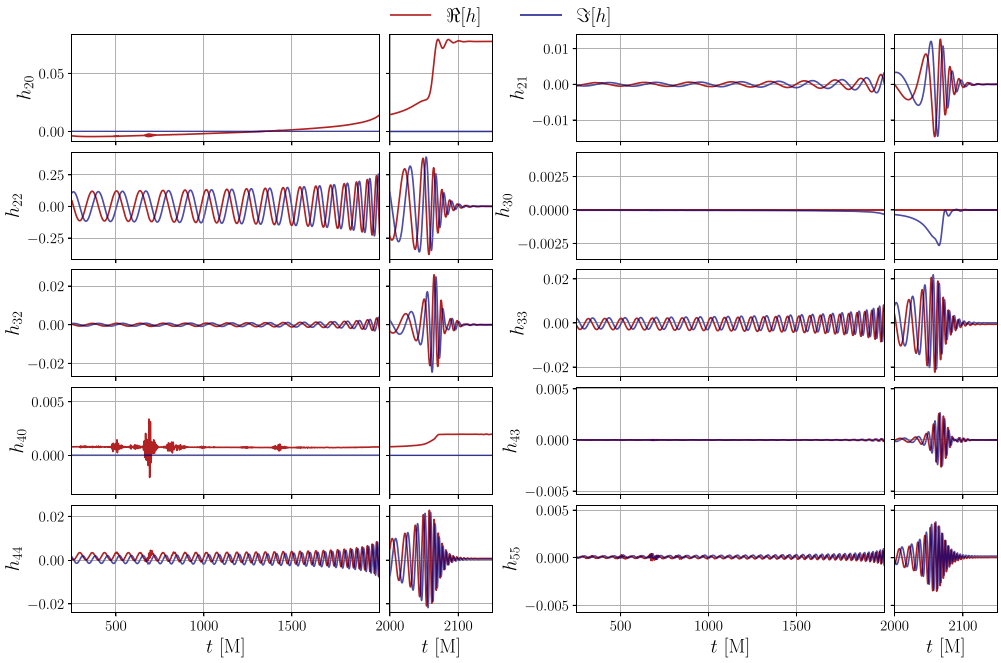

Figure 3. Real and imaginary parts of the waveform multipoles $h_{\ell m}$ extracted at $\mathcal{I}^+$ via CCE. Numerical noise is evident in the $(2,0),(4,0),(4,4)$ and $(5,5)$ modes around $t \simeq 700M$. Memory effects are also visible, particularly in the $m=0$ modes.

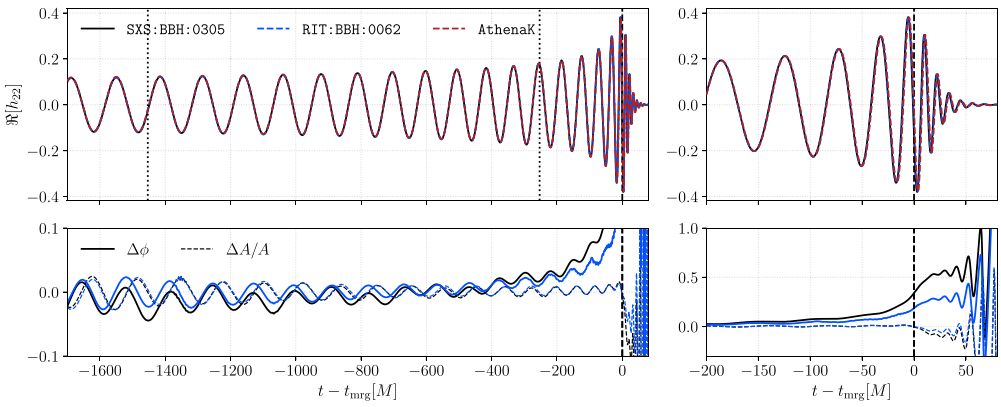

Figure 4. Comparison of the dominant $\ell = m = 2$ waveform multipole obtained from our targeted simulation (red dashed) against the same quantity from the `SXS:BBH:0305` (black) and `RIT:BBH:0062` (blue dashed) simulations. The phase and amplitude differences are reported in the bottom panel, and remain small throughout the entire evolution, with a maximum $\Delta\phi \sim 0.35$ and $\Delta A/A \sim 0.4\%$ around merger.

Table 1. Priors on intrinsic (M, ι) and extrisinc $(d_L, \psi, \phi_{\rm ref}, \alpha, \delta, t_{\rm c})$ parameters employed for the re-analysis of GW150914 with the `AthenaK` waveform modes.

Parameter name	Prior	Range
Total mass $M(M_\odot)$	Uniform	$[40, 100]$
Luminosity distance $d_{\rm L}$ (Mpc)	Uniform in source frame	$[50, 2000]$
Inclination ι (rad)	Sine	$[0, \pi]$
Polarization ψ (rad)	Uniform (periodic)	$[0, \pi]$
Reference phase $\phi_{\rm ref}$ (rad)	Uniform (periodic)	$[0, 2\pi]$
Right ascension α (rad)	Uniform (periodic)	$[0, 2\pi]$
Declination δ (rad)	Cosine	$[-\pi/2, \pi/2]$
Coalescence time $t_{\rm c}$ (s)	Uniform	$[t_0 - 6, t_0 + 2]$

is minimized. In the above, ϕ_X denotes the GW phase of the $(2, 2)$ mode obtained with the code $\mathrm{X} = \{\texttt{SpEC}, \texttt{LazEv}\}$. Qualitatively, the visual agreement among the waveforms is excellent throughout the entire coalescence. Quantitatively, the cumulative phase difference at merger $\Delta\phi$ amounts to ≈ 0.35 and 0.2 rad between the `SXS-AthenaK` and `RIT-AthenaK` waveforms, respectively. The amplitude relative difference, $\Delta A/A$, remains almost constant until merger, at a value $0.2\% - 0.4\%$ depending on the simulation considered. These values are comparable to those obtained by current state of the art models, calibrated to NR (see e.g. 1 of [122]).

3.3. Application to GW150914

The waveform multipoles $h_{\ell m}$ obtained via our targeted simulations can be used directly to estimate some of the source properties of GW150914. In particular, we can use the NR data to estimate source parameters that are extrinsic to the binary (sky position, orientation), because it is possible to sample over these parameters without generating new simulation data. Indeed, while mass ratio and (dimensionless) spins are set at the beginning of the simulation, the total mass M, inclination ι, reference phase $\phi_{\rm ref}$, polarization ψ, luminosity distance d_L , right ascension and declination α, δ can be freely varied to project the plus and cross polarizations $h_+, h_\times$ on the detectors:

$$h_+ - i h_\times = \frac{M}{d_L} \sum_{\ell m} h_{\ell m -2} Y_{\ell m} (\iota, \phi_{\rm ref}) \tag{2}$$

$$h = h_+ F_+ (\psi, \alpha, \delta) + h_\times F_\times (\psi, \alpha, \delta) \,, \tag{3}$$

where F_+ and $F_\times$ are the antenna pattern functions.

We then re-analyze GW150914 using the `bilby` parameter estimation library [123]. We consider $(2,0), (2,\pm2), (2,\pm1), (3,\pm3), (3,\pm2), (4,\pm4), (4,\pm3), (4,\pm2), (5,\pm5)$ waveform multipoles and sample over the parameters listed above using standard priors used in GW analysis, listed in table 1. We download data from the Gravitational Wave Open Science Center (GWOSC) [124, 125], consider 8 s around the time GPS of event $t_0 = 1126259462.391$ s and the frequency range $f \in [35, 896]$ Hz. Figure 5 shows the visual agreement of the reconstructed waveform and its uncertainty with the whitened detector data: our targeted simulation clearly captures the strain induced by the incoming GW signal. Figure 6, instead, displays the posterior distributions of chirp mass $\mathcal{M}$, luminosity distance d_L and inclination ι we obtain. We find $\mathcal{M} = 30.7^{+0.6}_{-0.5} M_\odot$, $d_L = 460^{+140}_{-140}$ Mpc, $\iota = 2.7^{+0.3}_{-0.4}$ rad. These results are consistent with estimates obtained using state-of-the-art semi-analytic waveform models [62, 126], albeit more constrained. This difference is readily explained by the fact that, in our analysis, the mass

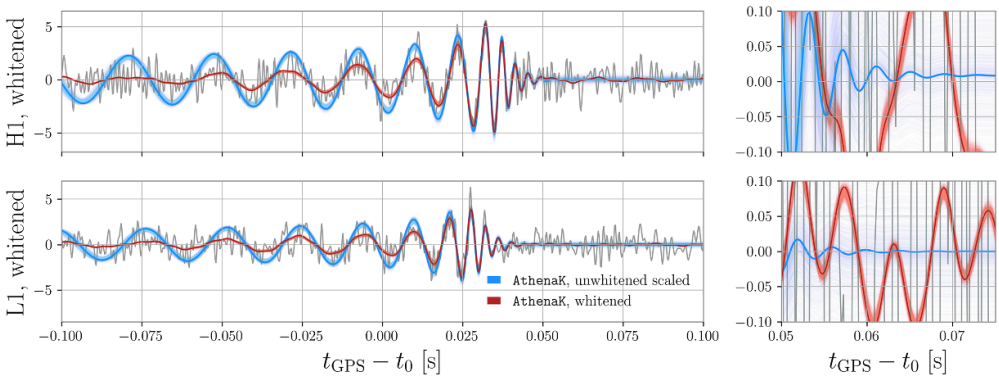

Figure 5. Reconstructed raw (blue) and whitened (red) waveforms, obtained performing PE with the modes $h_{\ell m}$ from the `AthenaK` simulation, overlaid to the whitened strain data from the Hanford (top) and Livingston (bottom) detectors around the time of GW150914, t_0. The dark red waveform corresponds to the maximum likelihood parameters; error bands around it are instead obtained considering 2000 waveforms from the analysis posterior, and are representative of the localization/mass uncertainty. The unwhitened waveform data clearly shows the impact of memory effects (right panels), with the polarizations not tapering to zero in H1.

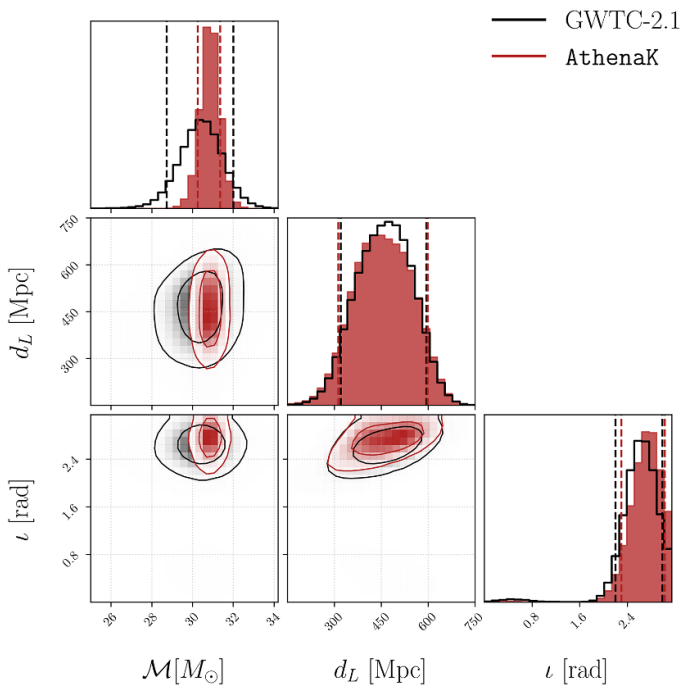

Figure 6. Posterior distribution of chirp mass $\mathcal{M}$, luminosity distance d_L and inclination ι recovered by analyzing the data of GW150914 using the waveform produced by our `AthenaK` simulation (red) compared to the full analysis of GWTC-2.1 performed with the `IMRPhenomXPHM` model [62, 127] (black). The estimates obtained from our simulation agree with those obtained from the semi-analytical model within 90% credibility.

ratio and component spins of the binary are fixed, thereby reducing the impact of parameter correlations.

4. Conclusions

We have revisited the BBH merger in GW150914 using the new, GPU-accelerated, NR code `AthenaK` [89–91]. This work serves as first cross-validation of `AthenaK` with established NR codes `LazEV` [17, 81] and `SpEC` [23, 30], as well as with real data. It also serves as demonstration of our pipeline for GW astronomy, which is made fully available to the community [95].

We have computed remnant properties using the isolated horizon formalism [119] and found excellent agreement with the `LazEV` and `SpEC` results presented in [80]. We have demonstrated the use of `AthenaK` world tube data in combination with `SpECTRE` [104] to compute GWs at $\mathcal{I}^+$ including memory effects, which were neglected in previous simulations of GW150914. We have found agreement between the dominant $(\ell, m) = (2, 2)$ mode of the GW signal obtained with this approach with previous results by [80], with flat residuals in amplitude and phase during most of the inspiral. The cumulative dephasing between `AthenaK` and `LazEV`/`SpEC` is of $\Delta\phi \simeq 0.2 - 0.35$ radians at merger, while the relative amplitude difference is of $\Delta A/A \simeq 0.2\% - 0.4\%$. Finally, we have applied our simulation to the analysis of real GW data, performing a parameter estimation study on GW150914. We found very good agreement with the previous results from the LIGO–Virgo–Kagra collaboration, estimating $\mathcal{M} = 30.7^{+0.6}_{-0.5} M_\odot$, $d_L = 460^{+140}_{-140}$ Mpc and $\iota = 2.7^{+0.3}_{-0.4}$ rad.

The main limitation of this work is that we have only considered a single grid resolution with `AthenaK`. Future work is also needed to address possible gauge effects in the waveform comparison between `AthenaK` and other codes. Work along these lines is already ongoing and will be reported in the future.

Data availability statement

The data that support the findings of this study are openly available at the following URL/DOI: https://github.com/dradice/athenak-tutorial-gw150914/.

Acknowledgment

We thank Zachariah Etienne for having provided us the minimal version of the `Einstein Toolkit` used for the black hole horizon analysis, and the `SpECTRE` developers for their assistance with `SpECTRE`'s Cauchy-characteristic extraction module. DR gratefully acknowledge the hospitality and support from Sorbonne Université, where part of this work was carried out. This work was supported by NASA through Awards 80NSSC21K1720 and 80NSSC25K7213, and by the National Science Foundation under Grant No. PHY-2020275 (Network for Neutrinos, Nuclear Astrophysics, and Symmetries (N3AS)). This research used resources of the Argonne Leadership Computing Facility, which is a DOE Office of Science User Facility supported under Contract DE-AC02-06CH11357. Computer time was provided by the INCITE program. Any opinions, findings, and conclusions or recommendations expressed in this material are those of the authors and do not necessarily reflect the views of the Department of Energy, NASA, or the National Science Foundation.

Appendix. Higher resolution simulation

In this section we validate the `AthenaK` data using results from a higher-resolution simulation, with otherwise identical setup. In particular, we perform an additional simulation with resolution of 192 points in the coarsest refinement level, as opposed to 128 of the baseline simulation. This results in a finest resolution of $\Delta_{192} = 0.0052083$**.**

The modes obtained from the higher-resolution simulation are presented in figure A1. Notably, differences among the two resolutions also impact the determination of the superrest frame of each binary. As such, some of the modes dominated by memory contributions, e.g. the $(\ell = 4, m = 0)$ mode, appear rather different as the resolution is increased. However, we obtain overall good agreement between the two resolutions in the phase and amplitude evolution of most of the modes. For example, the phase difference for the $(\ell = 2, m = 2)$ mode at merger is $\Delta\phi_{22} = 0.38$ and the relative amplitude difference is $\Delta A_{22}/A_{22} = 0.2\%$**.** Compared to the SXS (RIT) simulation shown in figure 4, this resolution achieves a phase difference of $\Delta\phi = 0.12$ (0.17) rad, and a relative amplitude difference of $\Delta A_{22}/A_{22} = 0.01\%$ (0.02%).

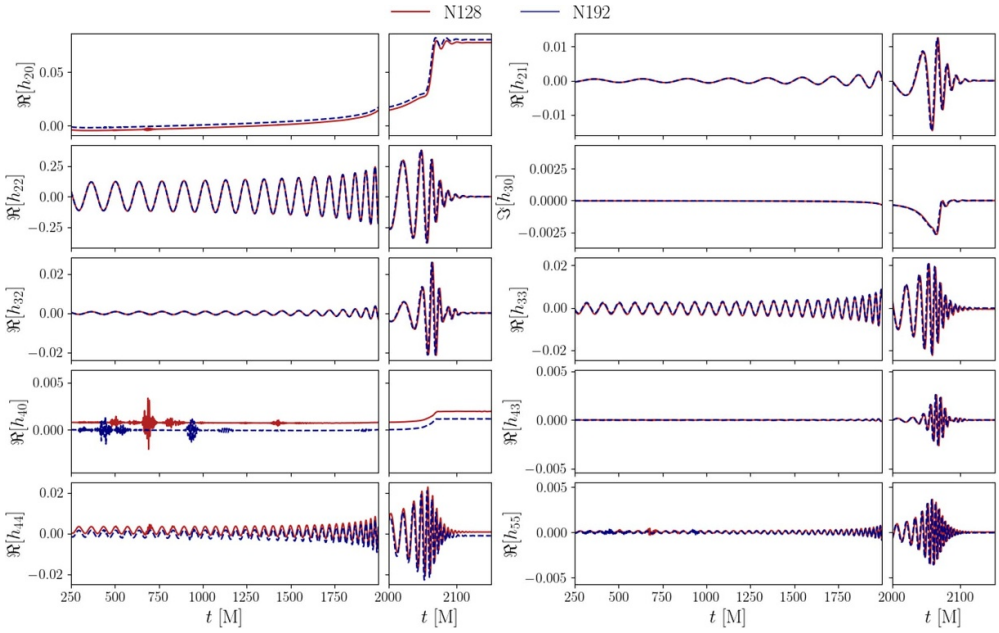

Figure A1. Real (or imaginary) parts of the waveform multipoles $h_{\ell m}$ extracted at $\mathcal{I}^+$ via CCE for the $N = 192$ simulation, compared to the lower resolution one with $N = 128$.

ORCID iDs

David Radice 0000-0001-6982-1008
Rossella Gamba 0000-0001-7239-0659
Hengrui Zhu 0000-0001-9027-4184
Alireza Rashti 0000-0003-3558-7684

References

[1] Abbott B P *et al* (LIGO Scientific and Virgo) 2016 *Phys. Rev. Lett.* **116** 061102
[2] Abbott B P *et al* (LIGO Scientific and Virgo) 2016 *Phys. Rev. Lett.* **116** 241102
[3] Abbott B P *et al* (LIGO Scientific and Virgo) 2016 *Astrophys. J. Lett.* **818** L22
[4] Abbott B P *et al* (LIGO Scientific and Virgo) 2016 *Phys. Rev. Lett.* **116** 221101
Abbott B P *et al* (LIGO Scientific and Virgo) 2018 *Phys. Rev. Lett.* **121** 129902 (erratum)
[5] Cardoso V, Franzin E and Pani P 2016 *Phys. Rev. Lett.* **116** 171101
Cardoso V, Franzin E and Pani P 2016 *Phys. Rev. Lett.* **117** 089902 (erratum)
[6] Yunes N, Yagi K and Pretorius F 2016 *Phys. Rev. D* **94** 084002
[7] Cardoso V and Pani P 2019 *Living Rev. Relativ.* **22** 4
[8] Cardoso V and Gualtieri L 2016 *Class. Quantum Grav.* **33** 174001
[9] Carullo G *et al* 2018 *Phys. Rev. D* **98** 104020
[10] Isi M, Giesler M, Farr W M, Scheel M A and Teukolsky S A 2019 *Phys. Rev. Lett.* **123** 111102
[11] Cotesta R, Carullo G, Berti E and Cardoso V 2022 *Phys. Rev. Lett.* **129** 111102
[12] Cabero M, Capano C D, Fischer-Birnholtz O, Krishnan B, Nielsen A B, Nitz A H and Biwer C M 2018 *Phys. Rev. D* **97** 124069
[13] Isi M, Farr W M, Giesler M, Scheel M A and Teukolsky S A 2021 *Phys. Rev. Lett.* **127** 011103
[14] Baumgarte T W and Shapiro S L 2010 *Numerical Relativity: Solving Einstein's Equations on the Computer* (Cambridge University Press)
[15] Smarr L, Cadez A, DeWitt B S and Eppley K 1976 *Phys. Rev. D* **14** 2443–52
[16] Pretorius F 2005 *Phys. Rev. Lett.* **95** 121101
[17] Campanelli M, Lousto C O, Marronetti P and Zlochower Y 2006 *Phys. Rev. Lett.* **96** 111101
[18] Baker J G, van Meter J R, McWilliams S T, Centrella J and Kelly B J 2007 *Phys. Rev. Lett.* **99** 181101
[19] Baker J G, Centrella J, Choi D-I, Koppitz M and van Meter J 2006 *Phys. Rev. D* **73** 104002
[20] Sperhake U 2007 *Phys. Rev. D* **76** 104015
[21] Bruegmann B, Gonzalez J A, Hannam M, Husa S, Sperhake U and Tichy W 2008 *Phys. Rev. D* **77** 024027
[22] Scheel M A, Pfeiffer H P, Lindblom L, Kidder L E, Rinne O and Teukolsky S A 2006 *Phys. Rev. D* **74** 104006
[23] Szilagyi B, Lindblom L and Scheel M A 2009 *Phys. Rev. D* **80** 124010
[24] Thierfelder M, Bernuzzi S and Bruegmann B 2011 *Phys. Rev. D* **84** 044012
[25] Loffler F *et al* 2012 *Class. Quantum Grav.* **29** 115001
[26] Babiuc M C, Szilagyi B, Winicour J and Zlochower Y 2011 *Phys. Rev. D* **84** 044057
[27] Hilditch D, Weyhausen A and Brügmann B 2016 *Phys. Rev. D* **93** 063006
[28] Bugner M, Dietrich T, Bernuzzi S, Weyhausen A and Brügmann B 2016 *Phys. Rev. D* **94** 084004
[29] Clough K, Figueras P, Finkel H, Kunesch M, Lim E A and Tunyasuvunakool S 2015 *Class. Quantum Grav.* **32** 245011
[30] Kidder L E *et al* 2017 *J. Comput. Phys.* **335** 84–114
[31] Daszuta B, Zappa F, Cook W, Radice D, Bernuzzi S and Morozova V 2021 *Astrophys. J. Supp.* **257** 25
[32] Rashti A, Bhattacharyya M, Radice D, Daszuta B, Cook W and Bernuzzi S 2024 *Class. Quantum Grav.* **41** 095001
[33] Daszuta B 2024 *J. Comput. Phys.* **508** 112958
[34] Rashti A, Gamba R, Chandra K, Radice D, Daszuta B, Cook W and Bernuzzi S 2025 *Phys. Rev. D* **111** 104078
[35] Buonanno A and Damour T 1999 *Phys. Rev. D* **59** 084006
[36] Buonanno A and Damour T 2000 *Phys. Rev. D* **62** 064015
[37] Ramos-Buades A, Buonanno A, Khalil M and Ossokine S 2022 *Phys. Rev. D* **105** 044035
[38] Pompili L *et al* 2023 *Phys. Rev. D* **108** 124035
[39] Ramos-Buades A, Buonanno A, Estellés H, Khalil M, Mihaylov D P, Ossokine S, Pompili L and Shiferaw M 2023 *Phys. Rev. D* **108** 124037
[40] Chiaramello D and Nagar A 2020 *Phys. Rev. D* **101** 101501
[41] Akcay S, Gamba R and Bernuzzi S 2021 *Phys. Rev. D* **103** 024014
[42] Gamba R, Akçay S, Bernuzzi S and Williams J 2022 *Phys. Rev. D* **106** 024020
[43] Nagar A, Rettegno P, Gamba R, Albanesi S, Albertini A and Bernuzzi S 2023 *Phys. Rev. D* **108** 124018

[44] Nagar A, Gamba R, Rettegno P, Fantini V and Bernuzzi S 2024 *Phys. Rev. D* **110** 084001
[45] Nagar A, Chiaramello D, Gamba R, Albanesi S, Bernuzzi S, Fantini V, Panzeri M and Rettegno P 2025 *Phys. Rev. D* **111** 064050
[46] Ajith P *et al* 2007 *Class. Quantum Grav.* **24** S689–700
[47] Ajith P *et al* 2008 *Phys. Rev. D* **77** 104017
Ajith P *et al* 2009 *Phys. Rev. D* **79** 129901 (erratum)
[48] Ajith P *et al* 2011 *Phys. Rev. Lett.* **106** 241101
[49] Santamaria L *et al* 2010 *Phys. Rev. D* **82** 064016
[50] Husa S, Khan S, Hannam M, Pürrer M, Ohme F, Jiménez Forteza X and Bohé A 2016 *Phys. Rev. D* **93** 044006
[51] Khan S, Husa S, Hannam M, Ohme F, Pürrer M, Jiménez Forteza X and Bohé A 2016 *Phys. Rev. D* **93** 044007
[52] Pratten G, Husa S, Garcia-Quiros C, Colleoni M, Ramos-Buades A, Estelles H and Jaume R 2020 *Phys. Rev. D* **102** 064001
[53] Estellés H, Ramos-Buades A, Husa S, García-Quirós C, Colleoni M, Haegel L and Jaume R 2021 *Phys. Rev. D* **103** 124060
[54] Estellés H, Colleoni M, García-Quirós C, Husa S, Keitel D, Mateu-Lucena M, Planas M d L and Ramos-Buades A 2022 *Phys. Rev. D* **105** 084040
[55] Hamilton E, London L, Thompson J E, Fauchon-Jones E, Hannam M, Kalaghatgi C, Khan S, Pannarale F and Vano-Vinuales A 2021 *Phys. Rev. D* **104** 124027
[56] London L, Khan S, Fauchon-Jones E, García C, Hannam M, Husa S, Jiménez-Forteza X, Kalaghatgi C, Ohme F and Pannarale F 2018 *Phys. Rev. Lett.* **120** 161102
[57] García-Quirós C, Colleoni M, Husa S, Estellés H, Pratten G, Ramos-Buades A, Mateu-Lucena M and Jaume R 2020 *Phys. Rev. D* **102** 064002
[58] Khan S, Ohme F, Chatziioannou K and Hannam M 2020 *Phys. Rev. D* **101** 024056
[59] Hannam M, Schmidt P, Bohé A, Haegel L, Husa S, Ohme F, Pratten G and Pürrer M 2014 *Phys. Rev. Lett.* **113** 151101
[60] Schmidt P, Ohme F and Hannam M 2015 *Phys. Rev. D* **91** 024043
[61] Khan S, Chatziioannou K, Hannam M and Ohme F 2019 *Phys. Rev. D* **100** 024059
[62] Pratten G *et al* 2021 *Phys. Rev. D* **103** 104056
[63] Blackman J, Szilagyi B, Galley C R and Tiglio M 2014 *Phys. Rev. Lett.* **113** 021101
[64] Blackman J, Field S E, Scheel M A, Galley C R, Hemberger D A, Schmidt P and Smith R 2017 *Phys. Rev. D* **95** 104023
[65] Varma V, Field S E, Scheel M A, Blackman J, Kidder L E and Pfeiffer H P 2019 *Phys. Rev. D* **99** 064045
[66] Varma V, Field S E, Scheel M A, Blackman J, Gerosa D, Stein L C, Kidder L E and Pfeiffer H P 2019 *Phys. Rev. Res.* **1** 033015
[67] Williams D, Heng I S, Gair J, Clark J A and Khamesra B 2020 *Phys. Rev. D* **101** 063011
[68] Hinder I *et al* 2014 *Class. Quantum Grav.* **31** 025012
[69] Jani K, Healy J, Clark J A, London L, Laguna P and Shoemaker D 2016 *Class. Quantum Grav.* **33** 204001
[70] Ferguson D *et al* 2023 arXiv:2309.00262
[71] Mroue A H *et al* 2013 *Phys. Rev. Lett.* **111** 241104
[72] Boyle M *et al* 2019 *Class. Quantum Grav.* **36** 195006
[73] Scheel M A *et al* 2025 arXiv:2505.13378
[74] Healy J, Lousto C O, Zlochower Y and Campanelli M 2017 *Class. Quantum Grav.* **34** 224001
[75] Healy J, Lousto C O, Lange J, O'Shaughnessy R, Zlochower Y and Campanelli M 2019 *Phys. Rev. D* **100** 024021
[76] Healy J and Lousto C O 2020 *Phys. Rev. D* **102** 104018
[77] Healy J and Lousto C O 2022 *Phys. Rev. D* **105** 124010
[78] Huerta E A *et al* 2019 *Phys. Rev. D* **100** 064003
[79] Hamilton E *et al* 2024 *Phys. Rev. D* **109** 044032
[80] Lovelace G *et al* 2016 *Class. Quantum Grav.* **33** 244002
[81] Zlochower Y, Baker J G, Campanelli M and Lousto C O 2005 *Phys. Rev. D* **72** 024021
[82] Nakamura T, Oohara K and Kojima Y 1987 *Prog. Theor. Phys. Suppl.* **90** 1–218
[83] Shibata M and Nakamura T 1995 *Phys. Rev. D* **52** 5428–44
[84] Baumgarte T W and Shapiro S L 1998 *Phys. Rev. D* **59** 024007
[85] Brandt S and Bruegmann B 1997 *Phys. Rev. Lett.* **78** 3606–9

[86] van Meter J R, Baker J G, Koppitz M and Choi D-I 2006 *Phys. Rev. D* **73** 124011
[87] Alcubierre M, Bruegmann B, Diener P, Koppitz M, Pollney D, Seidel E and Takahashi R 2003 *Phys. Rev. D* **67** 084023
[88] Lindblom L, Scheel M A, Kidder L E, Owen R and Rinne O 2006 *Class. Quantum Grav.* **23** S447–62
[89] Stone J M, Mullen P D, Fielding D, Grete P, Guo M, Kempski P, Most E R, White C J and Wong G N 2024 arXiv:2409.16053
[90] Zhu H, Fields J, Zappa F, Radice D, Stone J, Rashti A, Cook W, Bernuzzi S and Daszuta B 2024 arXiv:2409.10383
[91] Fields J, Zhu H, Radice D, Stone J M, Cook W, Bernuzzi S and Daszuta B 2025 *Astrophys. J. Suppl.* **276** 35
[92] Bernuzzi S and Hilditch D 2010 *Phys. Rev. D* **81** 084003
[93] Cao Z and Hilditch D 2012 *Phys. Rev. D* **85** 124032
[94] Stone J M *et al* (available at: https://github.com/IAS-Astrophysics/athenak)
[95] Radice D, Gamba R and Rashti A Binary black hole simulations with athenak (available at: https://github.com/dradice/athenak-tutorial-gw150914)
[96] Ansorg M, Bruegmann B and Tichy W 2004 *Phys. Rev. D* **70** 064011
[97] Bishop N T and Rezzolla L 2016 *Living Rev. Relativ.* **19** 2
[98] Reisswig C and Pollney D 2011 *Class. Quantum Grav.* **28** 195015
[99] Bishop N T, Gomez R, Lehner L, Szilagyi B, Winicour J and Isaacson R A 1998 *Cauchy Characteristic Matching* pp 383–408
[100] Reisswig C, Bishop N T, Pollney D and Szilagyi B 2009 *Phys. Rev. Lett.* **103** 221101
[101] Handmer C J and Szilagyi B 2015 *Class. Quantum Grav.* **32** 025008
[102] Moxon J, Scheel M A and Teukolsky S A 2020 *Phys. Rev. D* **102** 044052
[103] Moxon J, Scheel M A, Teukolsky S A, Deppe N, Fischer N, Hébert F, Kidder L E and Throwe W 2023 *Phys. Rev. D* **107** 064013
[104] Deppe N *et al* 2025 SpECTRE Simulating eXtreme Spacetimes (Zenodo) (https://doi.org/10.5281/zenodo.16906840)
[105] Boyle M, Iozzo D and Stein L C 2020 moble/scri: v1.2 (available at: https://doi.org/10.5281/zenodo.4041972)
[106] Boyle M 2013 *Phys. Rev. D* **87** 104006
[107] Boyle M 2016 *Phys. Rev. D* **93** 084031
[108] Boyle M, Kidder L E, Ossokine S and Pfeiffer H P 2014 arXiv:1409.4431
[109] Mitman K, Moxon J, Scheel M A, Teukolsky S A, Boyle M, Deppe N, Kidder L E and Throwe W 2020 *Phys. Rev. D* **102** 104007
[110] Magaña Zertuche L *et al* 2022 *Phys. Rev. D* **105** 104015
[111] Mitman K *et al* 2022 *Phys. Rev. D* **106** 084029
[112] Reisswig C, Bishop N T, Pollney D and Szilagyi B 2010 *Class. Quantum Grav.* **27** 075014
[113] Thornburg J 2004 *Class. Quantum Grav.* **21** 743–66
[114] Dreyer O, Krishnan B, Shoemaker D and Schnetter E 2003 *Phys. Rev. D* **67** 024018
[115] Haas R *et al* 2024 The Einstein Toolkit (available at: https://doi.org/10.5281/zenodo.14193969)
[116] Ruchlin I, Etienne Z B and Baumgarte T W 2018 *Phys. Rev. D* **97** 064036
[117] Tacik N *et al* 2015 *Phys. Rev. D* **92** 124012
Tacik N *et al* 2016 *Phys. Rev. D* **94** 049903 (erratum)
[118] Tichy W, Rashti A, Dietrich T, Dudi R and Brügmann B 2019 *Phys. Rev. D* **100** 124046
[119] Ashtekar A and Krishnan B 2004 *Living Rev. Relativ.* **7** 10
[120] Mitman K *et al* 2024 *Class. Quantum Grav.* **41** 223001
[121] Nichols D A 2017 *Phys. Rev. D* **95** 084048
[122] Gamba R, Lange J, Chiaramello D, Tissino J and Tibrewal S 2025 arXiv:2505.21612
[123] Ashton G *et al* 2019 *Astrophys. J. Suppl.* **241** 27
[124] Abbott R *et al* (LIGO Scientific and Virgo) 2021 *SoftwareX* **13** 100658
[125] Abbott R *et al* (KAGRA, VIRGO and LIGO Scientific) 2023 *Astrophys. J. Suppl.* **267** 29
[126] Ossokine S *et al* 2020 *Phys. Rev. D* **102** 044055
[127] Abbott R *et al* (LIGO Scientific and VIRGO) 2024 *Phys. Rev. D* **109** 022001